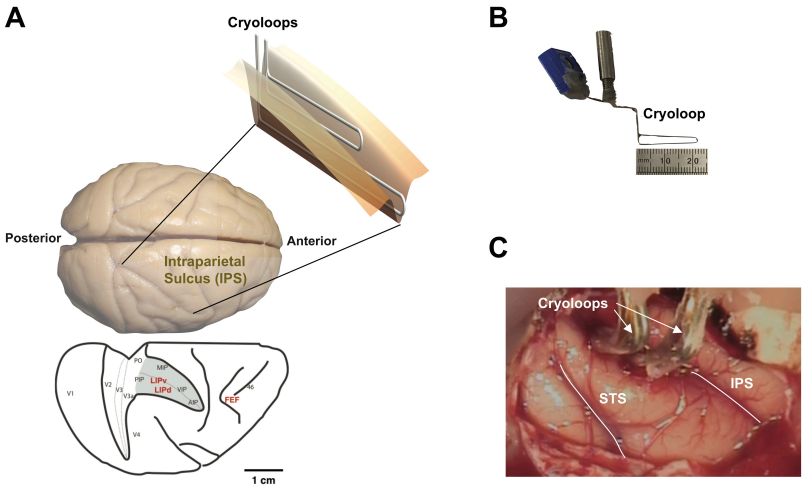

Figure S1. Implantation of cryoloops within the intraparietal sulcus (IPS), related to Figure 1. (**A**) Schematic depiction of unilateral placement of two cryoloops within the IPS. Bottom outline of the brain shows the IPS opened, and the adjacent opened lunate sulcus. Shaded region shows the location of the cryloop implant amidst the surrounding areas of PPC. (**B**) A single cryoloop custom-made to fit the full extent of the ventral half of the IPS. (**C**) Intra-operative photograph of cryoloop implants in monkey J. Image shows both ventral and dorsal loops situated within the IPS, and the loops emerging from the sulcus, as well as the nearby superior temporal sulcus (STS). PO, posterior occipital area; PIP, posterior intraparietal area; MIP, medial intraparietal area; VIP, ventral intraparietal area; AIP, anterior intraparietal area; LIPv, ventral aspect of lateral intraparietal area; LIPd, dorsal aspect of lateral intraparietal area.

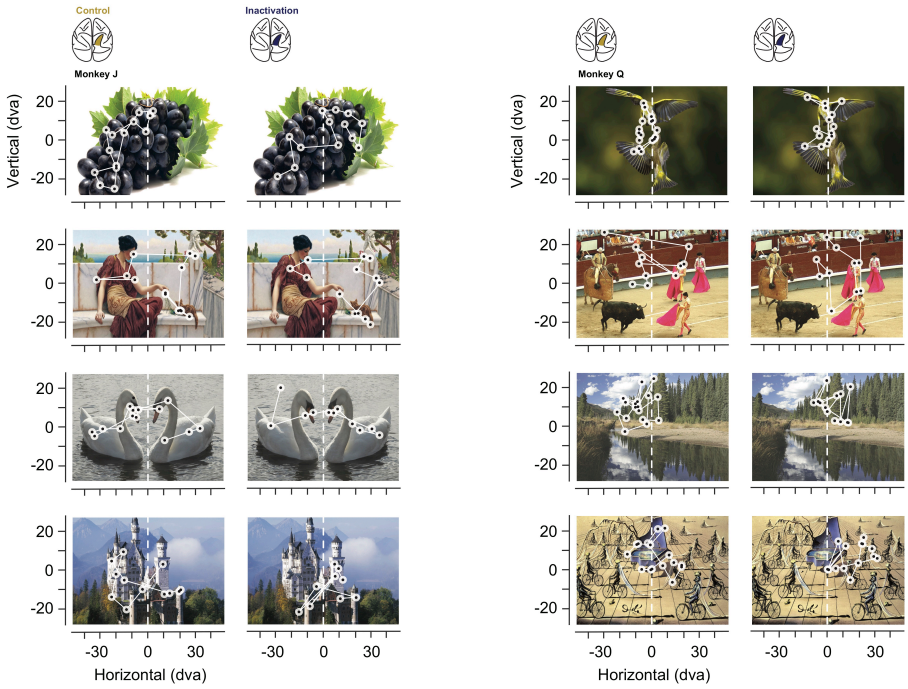

Figure S2. Free-viewing of images before and during parietal inactivation, related to Figure 1. Examples of images freely viewed by the two monkeys. Circles indicate regions of fixation and lines indicate saccades. For each monkey, control trials are shown on the left, and inactivation trials are shown on the right.

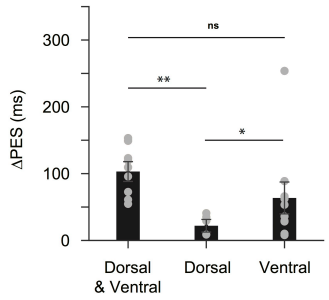

Figure S3. Behavioral effects of dorsal and ventral PPC inactivation, related to Figure 1. Comparisons of the shifts in double-target task effects during dorsal and ventral PPC inactivation in monkey Q. Bars show mean changes in PES values (inactivation – control) for sessions in which both dorsal and ventral cryoloops were cooled, or either the dorsal or ventral loops were cooled independently. Positive ΔPES values indicate a bias toward ipsilateral targets. Ventral cooling yielded effects comparable to cooling both dorsal and ventral loops and were more effective than dorsal cooling. Permutation was used for significance testing. Circles indicate data points from individual sessions. Error bars denote ±SEM; ns, not significant; *, $P < 0.05$; **, $P < 0.01$, paired t-test.

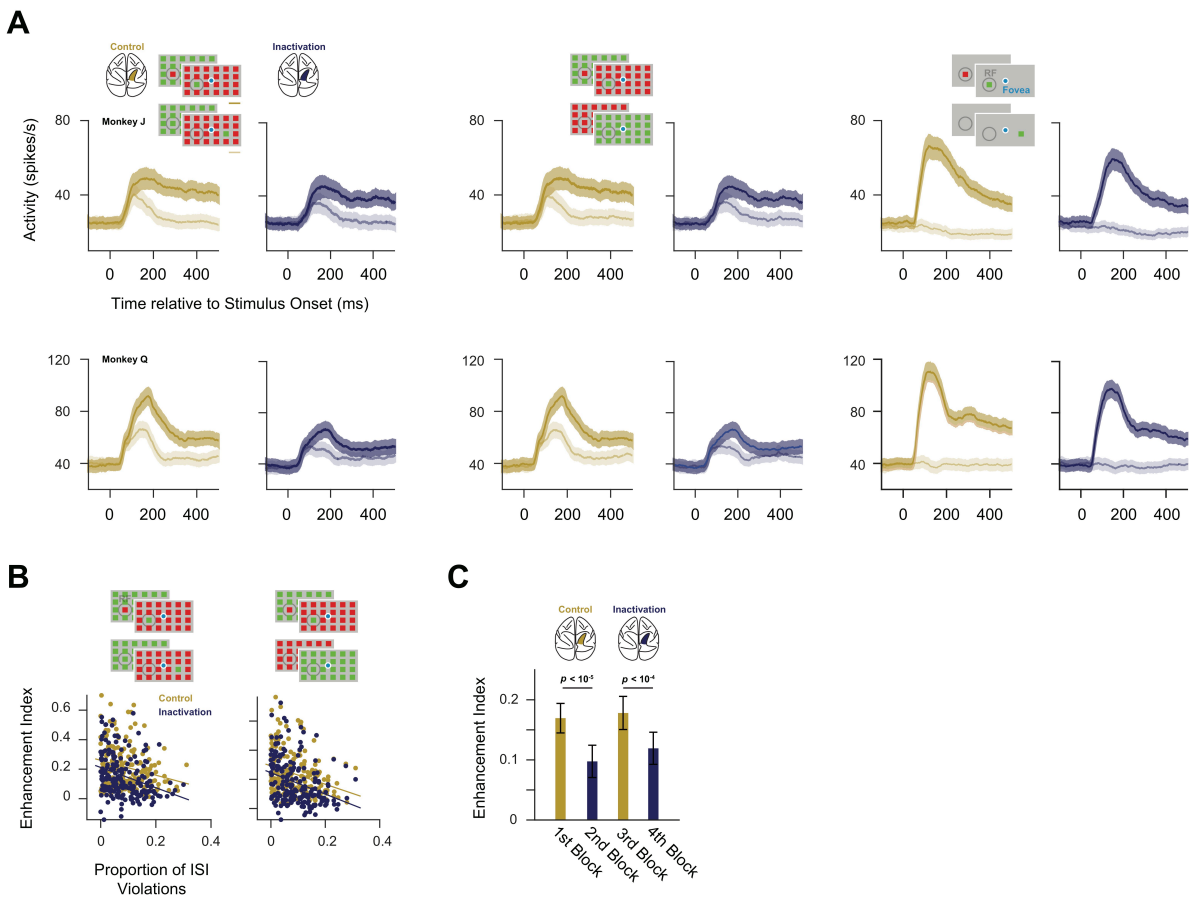

Figure S4. Representation of salience in prefrontal neuronal activity during PPC inactivation, related to Figure 4 (**A**) Mean responses for all modulated neurons to different stimulus conditions during control (gold) and PPC inactivation (blue) for the two animals (Monkey J, n = 92; Monkey Q, n = 101). Left, responses to $Unique_{In}$ (dark) and $Unique_{Out}$ (light) stimuli. Middle, responses to $Unique_{In}$ (dark) and Identical (light). Right, responses to the isolated stimuli presented inside (dark) and outside of the CRF (light). Shading around the response denotes ±SEM. (**B**) Enhancement indices for all modulated recordings (n = 193) as a function of inter-spike-interval (ISI) violations of clustered spike waveforms during control (gold) and inactivation (blue) blocks. The enhancement index was reduced during inactivation (Repeated Measures GLM, P = 0.002, P = 0.002), and decreased with increasing ISI violations (Repeated Measures GLM, $P < 10^{-}$

^{4}, $P < 10^{-6}$), but did so independently of the reduction in enhancement across control and inactivation blocks for both types of enhancement (Repeated Measures GLM, $P = 0.11$; $P = 0.25$, respectively), indicating that changes in recording quality did not contribute to the reduction in visual salience modulation during inactivation. (**C**) Mean enhancement indices across repeated sequences of control and inactivation blocks (control, gold; inactivation, blue). Error bars denote ±SEM. The observed reduction between the 1st and 2nd block was not significantly different from the reduction between the 3rd and 4th blocks (2 x 2 Repeated Measures ANOVA, $P = 0.40$).

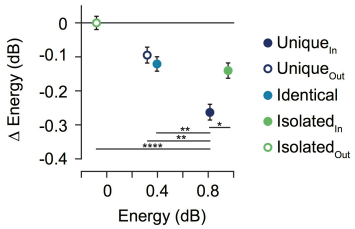

Figure S5. Changes in high-gamma band energy during PPC inactivation across different stimulus conditions, related to Figure 5. Points plot the mean high-gamma band LFP energy measured after the onset (0-500ms) of different visual stimuli. The reduction in high-gamma responses to unique stimuli in the URF was significantly larger than that of all other stimulus conditions ($Unique_{out}$: $p = 1.1 \times 10^{-3}$; $Isolated_{In}$: $p = 0.027$; $Isolated_{Out}$: $p < 10^{-5}$; Identical: $p=1.6 \times 10^{-3}$). Paired permutation was used for significance testing. Error bars denote ±SEM; *, $P < 0.05$; **, $P < 0.01$; ****, $P < 10^{-4}$.

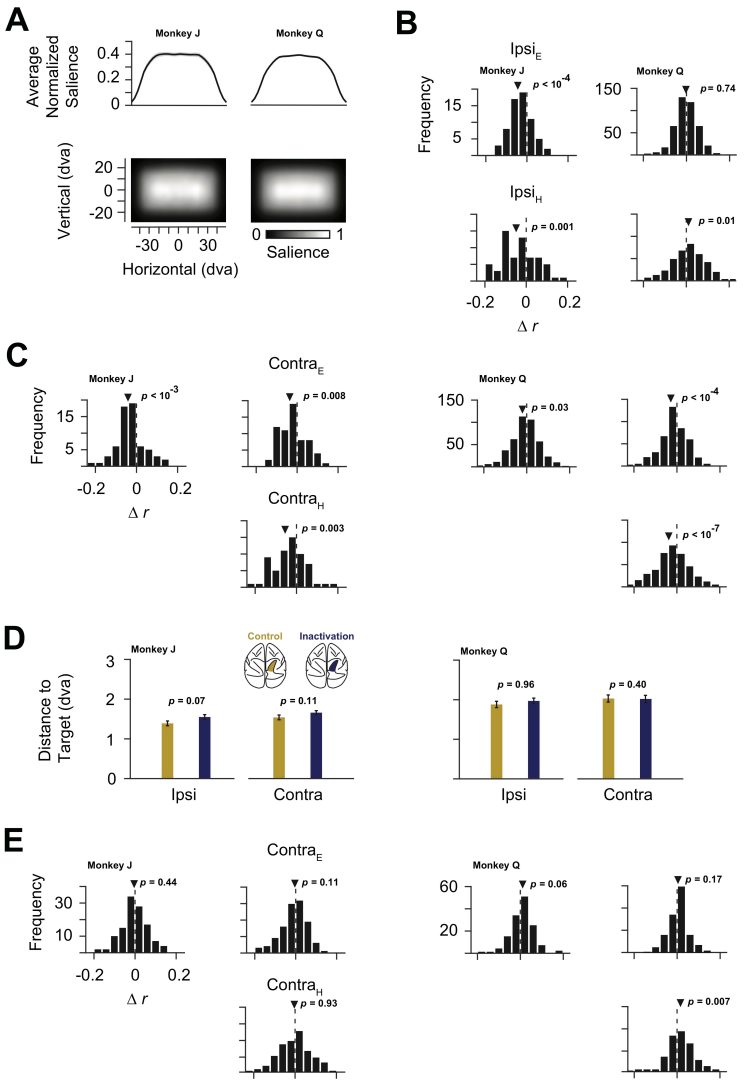

Figure S6. Eye-centered and head-centered changes in salience-driven fixations during PPC inactivation, related to Figure 6. (A) Distribution of salience across all images for Monkey J (left) and Monkey Q (right). Salience (GBVS model) was equally distributed within +/- 20 degrees across the horizontal dimension. (**B**) Distribution of changes in fixation-salience map correlation coefficients ($r_{\text{inactivation}} - r_{\text{control}}$) from ipsilateral fixations defined in eye-centered (Ipsi_E) (top) or in head-centered (Ipsi_H)(bottom) coordinates. Salience was computed using the GBVS model. (**C**) Distribution of changes in fixation-salience map correlation coefficients across the population of images for the two monkeys as computed with the Itti et al., 1998 salience model. The left

histogram for each monkey shows distributions based on coefficients measured from fixations across the full image. Right histograms for each monkey show distributions based on contralateral fixations, defined in eye-centered ($Contra_E$) or head-centered ($Contra_H$) coordinates. (**D**) Effect of PPC inactivation on the accuracy of saccades to single targets. Bar plots show the mean saccadic error (distance to target) during control and inactivation trials for both monkeys. PPC inactivation did not significantly alter saccadic error in either hemifield of the two monkeys. Target eccentricity was 10 dva for monkey J and 15 dva for monkey Q. Error bars denote ±SEM. (**E**) Distribution of changes in fixation-salience map (GBVS) correlation coefficients across the population of images for the two monkeys for two sequential (sham) control blocks. Same organization and notation as in C. Paired t-tests were used in statistical tests.

Table S1. Comparison of LFP energy between visual stimulus conditions for different frequency bands during control trials, related to Figure 2.

Frequency band	*M* (dB)	*SE*	*t*(191)	*P*
Isolated$_{In}$ vs Isolated$_{Out}$				
Alpha	1.436	0.161	8.903	$< 10^{-15}$
Beta	0.034	0.090	0.375	0.708
Gamma	0.244	0.070	3.507	$< 10^{-3}$
High gamma	1.052	0.058	18.065	$< 10^{-42}$
Unique$_{In}$ vs Unique$_{Out}$				
Alpha	0.107	0.134	0.799	0.425
Beta	-0.314	0.087	-3.607	$< 10^{-3}$
Gamma	0.136	0.067	2.038	0.043
High gamma	0.500	0.046	10.809	$< 10^{-20}$
Unique$_{In}$ vs Identical				
Alpha	-0.113	0.132	-0.860	0.391
Beta	-0.540	0.102	-5.308	$< 10^{-6}$
Gamma	0.125	0.064	1.963	0.051
High gamma	0.469	0.042	11.075	$< 10^{-21}$

LFP data were obtained after the onset [0-500) ms of different visual stimuli (n = 192 recordings). Paired t-test was used to test significance.

Table S2. Comparison of the reduction in visually driven activity across stimulus conditions during PPC inactivation, related to Figure 4.

	Intercept (spikes/s)	*P*	Slope	*P*
Average	0.88	0.01	-0.08	$< 10^{-35}$
Unique$_{In}$	1.10	0.75	-0.13	$< 10^{-4}$
Unique$_{Out}$	0.46	0.54	-0.06	0.14
Identical	1.42	0.43	-0.07	0.34
Isolated$_{In}$	-0.19	0.14	-0.10	0.29
Isolated$_{Out}$	1.60	0.28	-0.06	0.06

ANCOVA analysis examining the relationship between the change in visual activity during PPC inactivation (inactivation – control) and control visual activity across different visual stimulus conditions for all neuronal recordings (n = 352). Only the slope for the Unique$_{In}$ condition differed significantly from the overall average.